Journal of
Marine Science
and Engineering

MDPI

Article

Research on Structural Collapse of a Containership under Combined Bending–Torsion by Oblique Waves

Weiqin Liu [1,2], Qilu Zou [2], Yaqiang Zhang [2], Yong Nie [3,*] and Xuemin Song [1,2]

1 Key Laboratory of High-Performance Ship Technology, Ministry of Education, Wuhan University of Technology, Wuhan 430062, China; liuweiqin_123@sina.com (W.L.); sxmxs@whut.edu.cn (X.S.)
2 Department of Naval Architecture and Ocean Engineering, School of Naval Architecture, Ocean and Energy Power Engineering, Wuhan University of Technology, Wuhan 430062, China; zouqiluzql@163.com (Q.Z.); a330348703@gmail.com (Y.Z.)
3 China Harzone Industry Corp., Ltd., Wuhan 430204, China
* Correspondence: niehyung@163.com

Abstract: Large waves cause a great number of collapsed-ship accidents, resulting in the loss of many lives and properties. It has been found that most of these collapses are caused by encountering oblique waves. As a result, the ship structure experiences a complex collapse under combined bending and torsion. This paper utilizes a numerical hydroelasto-plastic approach, coupling CFD (Computational Fluid Dynamics) with the nonlinear FEM (Finite-Element Method), to study the structural collapse of a containership in oblique waves. First, a 4600 TEU containership was selected to study its collapse mechanism under oblique waves. Second, a hydroelasto-plastic numerical coupling of CFD and nonlinear FEM is used to co-calculate the wave loads and structural collapse of containership. The hydrodynamic model is constructed and used to solve wave loads in the CFD solver, and a nonlinear FEM model of containership with finer meshes is also modeled to solve the structural collapses, including plasticity and buckling. Third, several oblique-wave cases involving heading angles of 120°, 135°, 150°, and 180° are determined and calculated. Typical cases are discussed for time-domain stress histories and collapsed courses. Finally, the influence of oblique-wave parameters on structural collapse is discussed, and the collapse mechanism of containerships under the action of oblique waves is obtained, which provides a new understanding of ship structure design.

Keywords: containership; collapse; CFD; nonlinear FEM; oblique wave

check for updates

Citation: Liu, W.; Zou, Q.; Zhang, Y.; Nie, Y.; Song, X. Research on Structural Collapse of a Containership under Combined Bending–Torsion by Oblique Waves. *J. Mar. Sci. Eng.* **2024**, *12*, 444. https://doi.org/10.3390/jmse12030444

Academic Editor: Joško Parunov

Received: 25 December 2023
Revised: 26 January 2024
Accepted: 1 February 2024
Published: 1 March 2024

1. Introduction

1.1. Background of This Paper

Containerships have large openings on the deck, so it is necessary to evaluate their strength and collapse. When a containership with a large opening encounters a large oblique wave, the ship's structure will suffer the combined effect of a large bending moment and a large torsional moment induced by the pressures of the oblique waves. According to previous research [1,2], the ultimate strength of the ship's structure is decreased significantly by the combined effect of a bending moment and a torsional moment. Many ship accidents are caused by encountering large oblique waves.

Statistically, a total of 22 ship structural-collapse accidents induced by large waves occurred worldwide between 1969 and 1994, and about 542 people lost their lives [3]. Most ship-collapse accidents involve tankers, bulk carriers, and containerships. It is a common requirement to evaluate all sea-going ship structures. However, containerships have the largest deck openings, so they are the most typical sea-going ships that could be susceptible to collapse following a collision with large waves. The Japanese containership Comfort, which carried 7000 TEUs, was broken by waves and sank on the Asia–Europe route on 17 June 2013. The official investigation report revealed that the reason for this was that the ship encountered oblique waves [4]. The containership MSC NAPOLI collapsed in heavy seas, the ship's bottom generated cracks, and water entered the hull. The ship girder was broken into two strips and sunk [5]. In 2020, the Ukrainian bulk carrier ARVIN was broken into two strips after encountering large waves in the Black Sea. Three sailors died, and three sailors went missing. The wave that caused structural breakage was oblique [6]. Those ship structural-collapse accidents aroused the concerns of many researchers of ship mechanics.

When a ship encounters an oblique wave, there is a very antisymmetric wave-pressure distribution on the portside and starboard side; bending and torsional moments are generated, and they interact. The coupling effect of bending–torsional moments causes the interaction of longitudinal stress and shearing stress, and longitudinal ultimate strength and torsional ultimate strength are both reduced. The collapses of ship structures involving plasticity and buckling are generated if the containership encounters a large oblique wave and ship-breaking accidents appear. It is essential to study the ship-collapse mechanism under the combination of bending and torsional moments caused by oblique-wave action.

1.2. Research on the Collapsed Response of Ship Structure under Bending and Torsional Moments

Over the past few decades, the study of the collapse of ship structures under bending and torsional moments has primarily relied on structural mechanics. In the 1980s, the works of the Ostapenko group raised the important issue that torsion can reduce the longitudinal strength of a ship with a large deck opening when the vessel travels in oblique seas with high waves [7–9]. Pedersen [10] developed the beam theory to analyze the torsional bending response of a ship's hull. After years of development, structural model testing and the nonlinear finite-element method have become the main research methods, but the complex FSI (Fluid–Structure Interaction) effect has not been considered. Paik et al. [11] investigated the ultimate strength characteristics of a 4300 TEU containership hull under combined vertical bending and torsion and realized that torsion is not a sensitive component for the ultimate vertical bending moment in a normal operation, but the ultimate strength of ship hulls with low torsional rigidity can be affected significantly when the torsional moment is relatively large. Sun and Guedes Soares [12] performed a small-scale physical model testing the ultimate torsional strength of a ship-type box girder, showing that the structural design of ships with a large deck opening using the initial yielding criteria may be too conservative. Tanaka et al. [13] conducted ultimate strength tests on three 1/13-scale hull models under combined vertical bending and torsion, showing that torsion can significantly reduce ultimate hull girder bending capacity. Wang et al. [14] figured out a comparable scale model to evaluate the ultimate strength of typical very large containerships. They conducted a comprehensive analysis of longitudinal limit bending and torsion and proposed a similar theory, designing a scale model that accurately represented the gradual collapse behavior observed in real ships during ultimate strength model testing. Zhang et al. [15] investigated the ultimate strength of a sandwich-box girder under vertical bending and torsion and validated the accuracy of the numerical model by comparing the test results to the simulation results. Lee et al. [16] examined the ultimate strength characteristics of constructed hull structures in extremely large containerships. The researchers used the intelligent finite-element method to analyze the ultimate strength of hull beams in very large ships, considering the coupling of bending moment and torsional moment. Hu et al. [17] conducted a numerical study on the residual ultimate strength of box girders with crack damage under torsional and bending loads applied individually or in combination. The impact of crack length, location, and orientation angle on the residual ultimate strength of the box girder was analyzed using the nonlinear finite-element method.

The response to a ship's collapse under bending and torsional moments exhibits strong structural nonlinearity involving plasticity, instability, and buckling. Nonlinear FEM is used to solve the structural collapse of a ship. Hypothetical and constant bending and torsional moment are applied to the FEM model to obtain the collapses. But in fact, bending and torsional moments caused by oblique waves are dynamic and interactive. The FSI problem for a ship collapse is strongly nonlinear. Structural nonlinearities have not yet been combined with the hydrodynamics of waves to solve the collapse of a ship's structure under bending and torsional moments.

1.3. Hydroelastic Response of a Ship's Structure in Oblique Waves

A hydroelastic ship model is placed in a tank of oblique waves to capture the hydroelastic response considering bending–torsion moments. Hirdaris et al. [18], Senjanović et al. [19], and Senjanović et al. [20] intensively investigated the hydroelasticity of ships in waves using the frequency domain method. They focused on vertical bending, horizontal bending, and torsion, whereas Senjanović et al. [19] and Senjanović et al. [20] used beam theory coupled with a boundary element method. In conjunction with beam theory, Hirdaris et al. [18] used a three-dimensional finite-element model. Lin et al. [21] conducted an experimental study on the influence of asymmetric shock on hydroelastic responses under oblique-wave conditions. They discovered nonlinear bounce and lash responses and analyzed the high-frequency bending and torsional moments associated with these responses. Kim et al. [22] conducted an experimental study on wave motion and load of a containership model with no forward velocity in a $-120°$ oblique regular wave. It was confirmed that a steeper wave contributes to an increase in the higher-order harmonic components, including the slamming events in the bending moments measured. Ivo et al. [23] discussed the effects of shearing on bending and torsion, as well as that of a transverse bulkhead on hull stiffness, and proposed a hydrodynamic model in condensed form. Zhu et al. [24] conducted model tests in a towed tank and ocean basin to consider the natural frequencies of bending and torsional modes and estimated the influence of bending and torsional vibration on extreme response values in irregular waves. Kim et al. [25] used the finite-element method, employing one-dimensional beam elements, to simulate the structural domain of the ship model. This approach effectively accounted for the coupling effect between torsion and bending and warping deformation. Sun et al. [26] used the Ship's Three-Dimensional Motion Program (HSC) to predict short- and long-term wave loads for 5500TEU containerships and compared the calculated values of the current classification rules to 5500TEU containerships. Riesner et al. [27] introduced a time-domain numerical method to forecast a ship's higher-order springing in oblique waves, considering vertical and horizontal bending and nonuniform torsion.

Although the hydroelastic responses of ship models have been investigated in oblique waves numerically as well as experimentally for decades, the available structural collapse induced by large oblique waves has not begun. Ships' hydroelastic responses are classified as linear and elastic. The typical responses of collapse, including plasticity, instability, and buckling, cannot be generated in these research studies. If oblique waves become large enough, it is inevitable for the ship, and structural nonlinearities are caused. It is necessary to investigate the structural collapse of ships in large oblique waves imposing bending and torsional moments.

1.4. Hydroelasto-Plasticity Research of Ships in Large Waves

Hydroelasto-plasticity is an academic concept used to study ship structural collapse, including plasticity and buckling, by Masaoka at the earliest. Ship structural collapse is not considered a pure structural nonlinearity anymore. Wave condition and structural nonlinear response are both regarded as co-calculating FSI problems [28]. Numerical hydroelasto-plastic methods combining hydrodynamics and nonlinear structural dynamics were proposed to study structural collapses. Hydroelasto-plastic methods were classified into two kinds. One kind is the potential-flow hydroelasto-plastic method, which combines the potential-flow theory and structural nonlinear method. The other kind is the viscous-flow hydroelasto-plastic method, which is proposed to utilize combined CFD and nonlinear FEM.

Potential-flow hydroelasto-plastic methods, which combine potential-flow theory and structural nonlinear methods, have been extensively studied. Potential-flow theory is used for solving wave loads, while nonlinear structural methods considering plasticity or buckling are used to evaluate structural collapses. Masaoka et al. [28] established a structural analysis system to study the longitudinal collapse behavior of ships. The FEM was used to calculate the structural modeling domain of hull beams, and the nonlinear fluid force on the hull was calculated based on the Ursell–Tasai method. The nonlinear relationship between bending motion and curvature is used to represent the collapse behavior of the girder section. Xu et al. [29] proposed a numerical water elastoplastic method that combined the bar theory and a nonlinear hinge. They compared the numerical results with the results of a water elastoplastic model test to simulate the nonlinear bending moment of a ship in a single wave. Liu et al. [30] calculated wave pressure using a nonlinear bar-theory code and then interpolated it into the wet surface element of the finite-element model to analyze the structural response during the collapse. Potential-flow hydroelasto-plastic methods have two key shortages: the first is that nonlinearities of wave load, including slamming, wetness, and the large deformation of a wet surface, cannot be considered by potential-flow theory, and the second is that the potential-flow hydroelasto-plastic method is still a one-way FSI approach, and the two-way FSI effect cannot be considered.

The FSIs of CFD and nonlinear FEM are expected to apply to hydroelasto-plastic problems. First, the FSI method, combining CFD and linear FEM, is used to study structural hydroelasticity. Lakshmynarayanana et al. [31] studied the wave–body interaction of flexible floating bodies. They used the bidirectional coupling between Star-CCM+ and Abaqus to illustrate the application of FSI in determining the hydroelasticity of ship structures in waves. Pal et al. [32] conducted a comprehensive study of the elasticity of hull beams under extremely high wave loads by combining CFD and FEM with one-way coupling and two-way coupling. The above researchers used the FSIs of CFD and linear FEM that cannot calculate the structural collapse of s ship's structure involving plasticity, instability, and buckling. However, Liu et al. [33] carried out an attempt to couple CFD and nonlinear FEM to investigate the hydroelasto-plastic response of a scale ship model. One-way FSI and two-way FSI were both studied. It was found that two-way FSI is better than one-way FSI for solving the hydroelasto-plastic problem. The above hydroelasto-plastic research was confined to discussing the effect of heading waves on collapses. The effect of oblique waves was not investigated. Only scale models of ships were studied for their collapse by numerical hydroelasto-plastic methods. The collapsed mode of real-scale ship structures has not been discussed.

1.5. Objective of This Paper

This paper primarily investigates the structural collapse of ships under the influence of oblique waves, which aims to provide new insights into a ship's structural design. When a ship encounters an oblique wave, there is a highly antisymmetric wave-pressure distribution on the portside and starboard side of the ship. As a result, bending and torsional moments are generated and interact, leading to bending and torsional deformations. The combined effect of bending moment and torsion causes longitudinal stress and shearing stress to interact, leading to a reduction in both longitudinal and torsional ultimate strength. When a containership encounters a large oblique wave, it may experience structural collapse due to plasticity and buckling. This can lead to ship-breaking accidents. Therefore, it is essential to investigate the actual ultimate strength of a ship's structure when subjected to the combined effects of bending and torsional moments caused by oblique waves.

Based on the above research investigations, two key problems need to be solved.

(1) It is necessary to introduce the FSI approach to study the structural collapse of a ship's structure by oblique waves. Formerly, the structural collapse of a ship under bending and torsion has been studied just by employing structural mechanics. The hypothetical and constant bending and torsional moments are applied to the ship model to capture or calculate structural responses. However, the interaction of the bending moment and the torsional moment is a kind of dynamic alteration. The structural dynamic collapsed course is a strong nonlinear FSI (Fluid–Structure Interaction) problem. In dynamic collapse,

there is an interaction of strong wave-load nonlinearities and structural nonlinearities. It is essential to study the collapse of a ship's structure under bending and torsional moments using the FSI approach.

(2) A viscous-flow hydroelasto-plastic coupling CFD and nonlinear FEM is anticipated to address the 3D (three-dimensional) antisymmetric collapse of ship structures in large oblique waves. In particular, when considering the antisymmetric collapse of ship structures, it is important to utilize 3D hydrodynamic and structural dynamics. CFD models hydrodynamics using a 3D total fluid domain, allowing for the simulation of fluid nonlinearities such as slamming, green water, splashing, and the breakage of the free surface. Nonlinear FEM is utilized to solve nonlinear stiffness when a ship's structure collapses, and it can calculate the structural nonlinearities related to plasticity and buckling. Predictable results are expected when using a two-way FSI scheme to simulate the structural collapse of a ship's structure to oblique waves.

The novelty of this paper is its use of a two-way FSI combination of CFD and nonlinear FEM to investigate the structural collapse of a full-scale containership under an interactive combination of bending moment and torsional moment caused by oblique waves. Therefore, the above two problems need to be solved. Although it is common for a ship to collapse by rogue waves in the real ocean, this paper studies a ship's collapse through regular wave models. It is a complex, strongly nonlinear FSI problem for a combination of wave loads and ship collapse. The numerical approach of CFD and nonlinear FEM still needs a progressive course to study the combination of wave load and ship collapse, so this paper uses regular waves to cause ship collapse. A full-scale 4600 TEU containership has been selected for the study of its structural-collapse mechanism in oblique waves. A hydroelasto-plastic numerical approach that couples CFD and nonlinear FEM is employed to simultaneously calculate wave loads and structural collapse. A hydrodynamic CFD model has been developed to solve the 3D antisymmetric wave pressure on a ship's body in oblique waves using a CFD platform. Additionally, a FEM model of a containership with finer meshes is constructed to solve structural collapses. Several oblique-wave cases with heading angles of 120°, 135°, 150°, and 180° are determined and calculated. Typical cases of time-domain stress histories are then discussed, with particular emphasis on the collapsed course of containerships. Finally, the impact of oblique-wave parameters on structural collapse is investigated, and the mechanism of containership collapse in oblique waves is analyzed. This paper aims to provide new insights into ship structural design.

2. Numerical Methodology

In this paper, the collapse of containership structures under oblique-wave action using a numerical hydroelasto-plastic method combined with CFD and nonlinear FEM has been studied. The wave load is calculated using CFD, and the FEM is employed to analyze problems such as plasticity and buckling in ship structures. In the following section, the fundamentals of CFD, FEM, and the combination of CFD to FEM (two-way CFD–FEM coupling) are discussed in detail.

2.1. Computational Fluid Dynamics

This paper uses the hydrodynamic solver STAR-CCM+, based on the Finite Volume Method (FVM), to calculate the water pressure on a ship structure under wave action. The FVM, based on the theory of viscous flow, discretizes the spatial fluid domain into small-scale control volumes. It assumes that the flow of fluid in space, within each small-scale control volume, is governed by the Continuity Equation and the Momentum Equation.

The Fluid Continuity Equation states that the increase in mass of a microelement in the flow field during a given time interval is equal to the net mass flowing into the microelement during that interval. Considering the motion of a ship in waves, seawater is considered to be an incompressible fluid, meaning that density does not change over time. Therefore, the Fluid Continuity Equation can be reduced to the following equation:

$$\frac{\partial(\rho u)}{\partial x} + \frac{\partial(\rho v)}{\partial y} + \frac{\partial(\rho w)}{\partial z} = 0 \tag{1}$$

where ρ is the density of the fluid, u, v, w are, respectively, the partial velocities in x, y, and z directions in the Cartesian coordinate system.

In viscous-flow theory, the Momentum Conservation Equation, also known as the Navier–Stokes Equation, is utilized. From the perspective of computational cost and flow field grid requirements, the paper adopts the RANS (Reynolds-Averaged Navier–Stokes) method to solve turbulent flow. The concept behind the RANS method is to time-average the N–S equations and separate velocity and pressure into mean values and fluctuations. The RANS equation, derived from the N–S equation, is described as follows:

$$\frac{\partial \overline{u_i}}{\partial t} + \overline{u_j}\frac{\partial \overline{u_i}}{\partial x_j} + \frac{\partial u_i' u_j'}{\partial x_j} = -\frac{1}{\rho}\frac{\partial \overline{p}}{\partial x_i} + v\frac{\partial^2 \overline{u_i}}{\partial x_j \partial x_j} + f_i \tag{2}$$

where i, j is the velocity component, f_i is the mass force, $\overline{u_i}$, $\overline{p}$ is the value of time average, and ${u_i}'$, p' is the pulsation value.

A numerical tank is built to simulate a realistic numerical environment in CFD. Waves are generated by the velocity input method. The porous medium method is utilized to absorb the reflected wave, therefore preventing a decrease in wave precision caused by the generation of reflected waves. Given the nonlinear effect of wave load, the Volume of Fluid (VOF) method is employed to capture the gas–liquid interface precisely. The phase volume fraction is used to determine the distribution and position of the interface between phases, which can be defined as follows:

$$a_i = \frac{V_i}{V} \tag{3}$$

where V_i is the volume of phase i in a meshed element, V is the volume of a whole meshed element. $0 < a_i < 1$ means that there are interfaces of multiple phases, which $a_i = 1$ means that the corresponding mesh element is filled by a single phase.

2.2. Nonlinear FEM

The collapse of ship structures involves geometric nonlinearity, material nonlinearity, and boundary condition nonlinearity. This paper uses the FEM software ABAQUS 2020 to discretize the structure and solve the nonlinear equations into which nonlinear problems of these structures are transformed.

Since damping exists in the actual case, it is usually added in the form of Rayleigh damping, the basic equation of structural dynamics of which is shown as follows:

$$[M]\{\ddot{u}\} + [C]\{\dot{u}\} + [K]\{u\} = \{F(t)\}_i \tag{4}$$

$$[C] = \alpha[M] + \beta[K] \tag{5}$$

where the first term on the left is the inertial force, the second and third term is the internal force, and the right term is the external force. $[M]$, $[C]$, $[K]$ are structural mass matrix, damping matrix, and stiffness matrix, $\ddot{u}$, $\dot{u}$, u are the acceleration, velocity, and displacement at the same time, α, β is the damping coefficient.

Due to the lengthy calculation time required for the entire fluid–structure coupling process and the need to input transient loads at each time step, the implicit dynamic algorithm will be used to solve the equation. The implicit dynamic algorithm adopts the Newton–Raphson method for iterative calculation [34], and its calculation process is shown in Figure 1. First, the external force P is decomposed into several increments and loaded onto the structure. According to the stiffness matrix coefficient K_1 in the initial state, the displacement δ_1 of the first incremental load P_1 is directly obtained by applying Hooke's Law:

$$\delta_1 = \delta_0 + \frac{P_1}{K_1} \tag{6}$$

Due to the underestimation of the initial system stiffness coefficient, there will be residual stress value under displacement at this time, which can be obtained by subtracting from the internal force of the structure:

$$R_1 = P_1 - P(\delta_1) \tag{7}$$

The new equivalent stiffness matrix K_2 under displacement δ_1 can be calculated, and the total displacement δ_2 after residual force R_1 is applied can be obtained:

$$\delta_2 = \delta_1 - \frac{R_1}{K_2} \tag{8}$$

Next, the new residual force R_2 and the new stiffness matrix K_3 are calculated and iterated repeatedly until the allowable error is satisfied and the result of the first incremental step is obtained. The next incremental force is continually applied, and the process is repeated until the end.

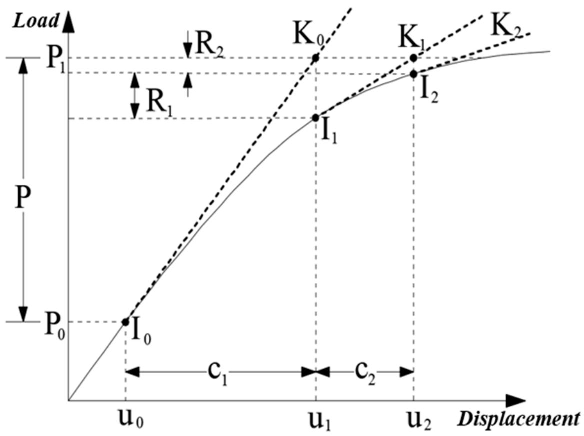

Figure 1. Newton–Raphson iterative method.

2.3. Two-Way FSI Coupling CFD and Nonlinear FEM

There is a strong interaction between the fluid load and structural response during the collapse of a ship's structure. Therefore, the reaction of a structure to collapse is a complex nonlinear fluid–structure coupling problem. Liu et al. [23] attempted to integrate CFD and nonlinear FEM to study the hydroelasto-plastic response of a scaled ship model. They investigated both one-way FSI and two-way FSI and concluded that two-way FSI is more effective than one-way FSI in addressing hydroelasto-plastic problems. In this study, the two-way coupling simulation function between the CFD software STAR-CCM+ 2021 and the nonlinear finite-element software ABAQUS 2020 was utilized to simulate wave load and transfer structural deformation through implicit coupling. The principle of this coupling is illustrated in Figure 2.

In a single iteration step of implicit coupling, ABAQUS first calculates the initial displacement value at time tn + 1 based on the initial flow field value. The initial estimate is then transferred to STAR-CCM+ using the specified fluid–structure coupling interface to finalize the deformation and movement. Finally, it solves the flow field to obtain the flow distribution at time tn + 1. The flow field value is then transferred back to ABAQUS to solve the structural response at time tn + 1. Next, the resolved structural displacement was transferred back to the flow field at time tn + 1 in STAR-CCM+. The iterative coupling calculation is repeated until the solution converges.

Within each time step of coupling, there are three complete exchanges of information, including wave pressure (P), inertia forces (I), motion (M), and deformation (D) generated by the hull structure. During the process, the convergence of the cubic internal iteration is achieved. At this time step, the flow field information and structural response are obtained.

Then, it will move on to the next coupling time step and calculate simultaneously until the end time is reached.

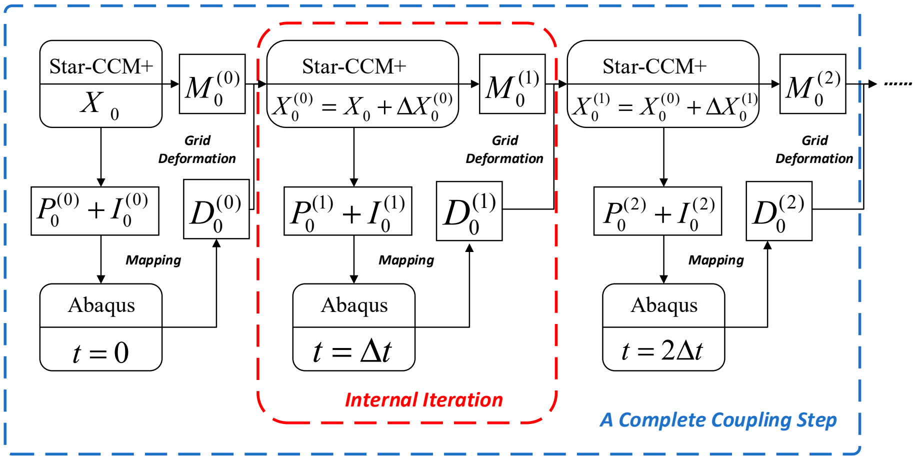

Figure 2. Schematic diagram of the two-way coupling method.

3. Numerical Modeling of Containership

A full-scale 4600 TEU containership was selected for modeling and calculation based on the numerical hydroelasto-plastic approach. The main dimensions of a 4600 TEU containership are presented, and the CFD model and FEM model are both established and discussed.

3.1. Description of a 4600 TEU Containership and Wave Cases

A full-scale 4600 TEU containership has been selected to study its structural collapse in oblique waves. The containership is a common ocean-going vessel. The containership selected in this paper has three large open cargo holds between the bridge and forecastle, and the structure design is a double-bottom and double-sided design. The main dimensions of the containership are given in Table 1. The overall length is 260 m, and the maximum displacement is 64,650 t. There are 3 holds to load containers with large deck openings, and strong, watertight transverse bulkheads compartmentalize the holds. A 3D model of a 4600 TEU containership without superstructure and forecastle is shown in Figure 3.

Table 1. Main dimensions of 4600 TEU containership.

Main Dimensions	Values
Overall length	260 m
Length between perpendiculars	245 m
Molded breadth	38 m
Molded depth	19.6 m
Designed draft	11 m
Displacement	64,650 t

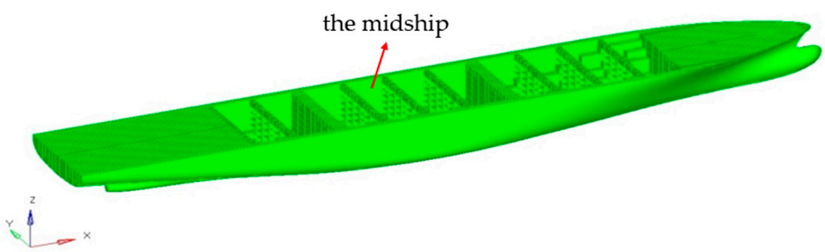

Figure 3. 4600 TEU Containership.

The structural collapse of a 4600 TEU containership in oblique waves will be studied in this paper, so several oblique heading angles and cases have been determined. All wavelengths are equal to 245 m, and the ratios of wavelength and ship length are kept to 1.0. Wave heights and wave heading angles are changed. Wave heights are 5 m, 9 m, and 16 m, while wave heading angles are determined to be 120°, 135°, 150°, and180°. The wave heading angle is the angle between the ship length and wave direction, as Figure 4 shows. A total of 10 wave cases are given in Table 2. Wave cases of H1, H2, and H3 have 5 m, 9 m, and 16 m wave heights, respectively, while other wave parameters are the same. In other wave cases, Ai-j, A1, A2, and A3 mean wave angles of 150°, 135°, and 120°, and Ai-1, Ai-2, and Ai-3 mean different wave heights of 5 m, 9 m, and 16 m.

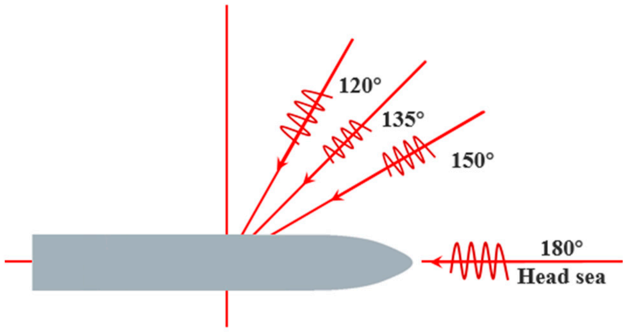

Figure 4. Oblique heading angles of the ship in this study.

Table 2. Wave cases of this research.

Case	Wavelength (m)	Wave Height (m)	Heading Angle (°)	Wavelength/Ship Length	Wave Steepness
H1	245	5	180	1	0.0204
H2	245	9	180	1	0.0367
H3	245	16	180	1	0.0653
A1-1	245	5	150°	1	0.0204
A1-2	245	9	150°	1	0.0367
A1-3	245	16	150°	1	0.0653
A2-1	245	5	135°	1	0.0204
A2-2	245	9	135°	1	0.0367
A2-3	245	16	135°	1	0.0653
A3-3	245	16	120°	1	0.0653

3.2. CFD Model of 4600 TEU Containership

A CFD model of a 4600 TEU containership has been constructed to calculate wave loads of containership and co-solve with a FEM solver. First, a calculating domain, including a ship model, an overlapping grid, a water-background grid, and an air-background grid, is meshed, as Figure 5 shows. The length of the calculating domain is 7 times the ship length, and the width of the calculating domain is double that of the ship length. An adjacent overlapping-grid region whose length is equal to 350 m is used to simulate the ship's motion by means of DFBI (Dynamic Fluid Body Interaction).

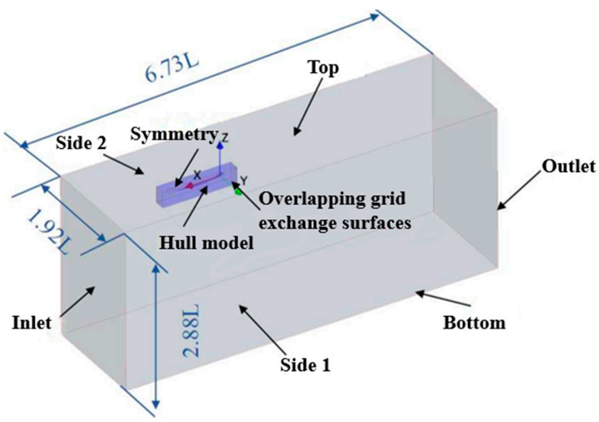

Figure 5. CFD model of a 4600 TEU containership.

This research meshes applicable grids to carry out CFD calculations. The probable size of the grid is determined to be 0.5 m, which is similar to FEM meshes to promote the smoothness of FSI. According to the requirement of simulating regular waves by ITTC [35], the number of grids is more than 40 within the range of wavelength, and the grid number is not less than 20 within the range of wave height. This study meshes 80 grids in a wavelength and 20 grids in wave height. The wave stability, fluid surface breaking, slamming, and green water can be captured; the final grid figure is shown in Figure 6. To determine the appropriate grid size and number, this study carries out a grid-independence analysis. Three typical grid cases are proposed to determine the final grid size: Case A of a fine grid has 11.44 million grids, Case B of a medium grid produces 6.55 million grids, and Case C of a coarse grid has 2.51 million grids. A wave-making calculation is executed to compare their numerical wave heights with theoretical wave heights. The grid size and computational results are given in Table 3, and the time-domain wave elevation is presented in Figure 7. It is found in Table 3 and Figure 7 that Case A and Case B have similar simulated wave heights, while Case C has a large error of 10.11%. However, Case A has a huge computational cost and grid number. Hence, Case B, with a grid number of 6.55 million, is an appropriate grid scheme in view of grid number as well as computational efficiency. The final grid number is determined to be 6.55 million for all CFD calculations in this study.

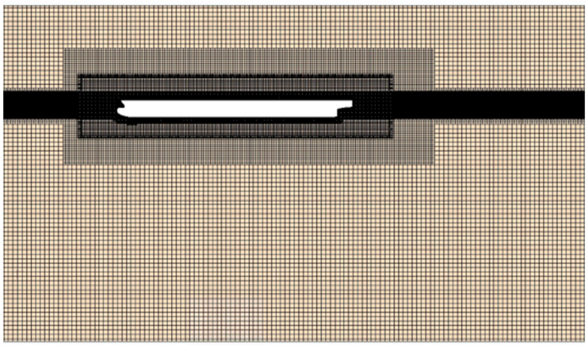

Figure 6. Grids of containership.

Table 3. Number size of CFD grids.

Grid Case	Grid Number	Errors
Case A (Fine grid)	11446884	1.11%
Case B (Medium grid)	6555065	2.12%
Case C (Coarse grid)	2512584	10.11%

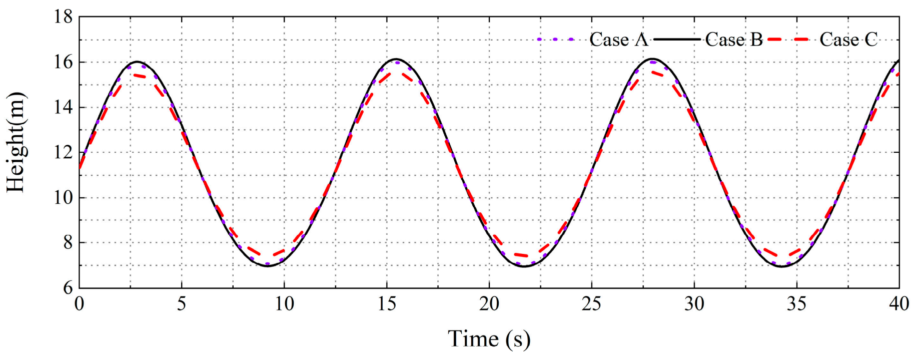

Figure 7. Wave elevation of 3 three typical grid cases.

3.3. Nonlinear FEM Model of 4600 TEU Containership

The FEM model of the 4600 TEU containership structure is modeled by the pre-treated software HYPERMESH 2019. The meshes of the FEM model are kept to appropriate sizes, which are small enough to simulate a buckling collapse. The structures below the main deck are modeled, and the total element number of the whole ship structure reaches 432,970. The FEM model of the whole ship structure is given in Figure 8. It can be seen that there are 3 holds. The starboard and port side are both constructed to investigate the asymmetric wave loads and structural collapse across the whole breadth. The structural material is determined to be Q235 steel, and its material parameters are given in Table 4. The yield stress is 235 MPa, and the ideal elasto-plastic constitutive relation is used in a nonlinear FEM solution.

Table 4. Material parameters of the FEM model.

Density (t/m^3)	Elastic Modulus (MPa)	Poisson's Ratio	Yield Strength
7850	2.06×10^5	0.33	235

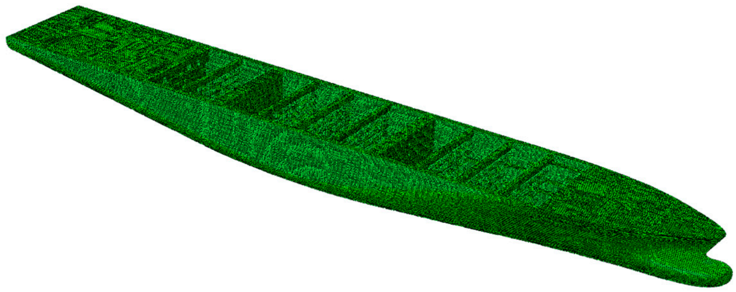

Figure 8. FEM model of the 4600 TEU containership.

To ensure that the error caused by the singularity of the stiffness matrix will not be reported in the calculation process of the container hull model and to avoid the longitudinal and transverse drift of containership under the action of inclined waves, it is necessary to set certain boundary conditions. In this paper, the bidirectional coupling calculation process limits the longitudinal and lateral drift of containerships and keeps the rolling angle of the container in a small angle range, which has a negligible effect on the wave direction angle. During the entire numerical simulation, only the pitch motion, heave motion, roll motion, and small-amplitude yaw motion of the model are released.

Generally, structural damage occurs in the midship area. Therefore, the nonlinear finite-element method is used to analyze the ultimate bending and ultimate torsional moments in the middle of the ship, and the ultimate bearing capacity and corresponding angle of the ship structure under vertical deformation, arch deformation, and torsion deformation are obtained. In the numerical simulation calculation, the corresponding reference points are set in the middle and axis positions of the end faces of the two end sections, and then the corresponding reference points are bound with the nodes of the end faces of the two ends by applying the MPC beam constraint, in which reference points are taken as the active points, and the end nodes are taken as the slave points. Finally, the final bending moment and angle results are obtained using the arc length method by applying torque to the reference points. The total longitudinal and torsional ultimate strength of the midship section can be confirmed, as shown in Figure 9. The bending angle–bending moment curve is shown in Figure 9a. The bending angle means the ship's bending rotational deformation, which generates longitudinal bending strength and bending moment. The torsional angle–torsional moment curve is presented in Figure 9b. The torsional angle means the torsional angle around the x-axis. The ultimate sagging bending moment is 3.09×10^9 N·m at an angle of 0.2232°, and the ultimate hogging bending moment is 4.37×10^9 N·m at an angle of $-0.2836°$. The ultimate torsional moment is 2.66×10^9 N·m when the torsional angle is 0.2929°.

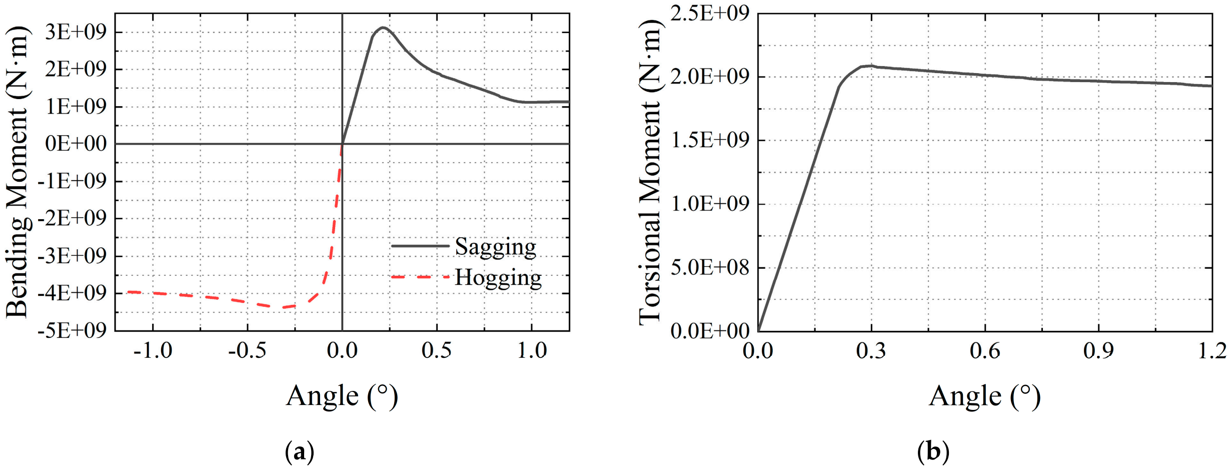

Figure 9. Curves of angle-bending moment/torsional moment. (**a**) Curve of bending angle-bending moment. (**b**) Curve of torsional angle-torsional moment.

4. Time-Domain Hydroelasto-Plastic Response Analyses

This paper focuses on the collapse characteristics of different wave directions. Therefore, this section only presents the time-domain results for collapse conditions at 120°, 135°, 150°, and 180°. The numerical hydroelasto-plastic approach, combining CFD and nonlinear FEM, involves strong nonlinearities and two-way FSI (Fluid–Structure Interaction). This method incurs high costs and requires lengthy calculation times. The collapse of the ship structure occurs within a very brief moment, and a 40-s simulation can include 3 cycles, which is adequate for simulating the collapse of the ship's structure. A total of 10 cases are simulated to study the time-domain structural collapses of a containership. It takes about 72 h to calculate the FSI solution by means of CFD and nonlinear FEM for every case.

4.1. Time-Domain Bending Angle and Torsional Angle

The time-domain numerical hydroelasto-plastic method combining CFD and nonlinear FEM is used to simulate all cases given in Table 2. In this paper, a time duration of 40 s is used for all simulations. The structural collapse of a ship structure happens very transiently, so the 40-s time duration, including 3 periods of waves, is enough to simulate the structural collapse of the ship.

Four oblique-wave cases, namely H3 (180°), A1-3 (150°), A2-3 (135°), and A3-3 (120°), were selected to study the structural collapse of a 4600 TEU containership in oblique waves. Under the conditions of inclined wave collapse, the ship undergoes periodic heaving, pitching, and deep rolling, as well as significant overall vertical bending and torsional deformation. The overall vertical bending deformation is reflected by the results of the time curve of the relative vertical bending deformation angle at the bow and stern, and the torsion deformation is reflected by the results of the relative torsion angle at the bow and stern.

Figure 10 shows the history of midship vertical bending angle in the wave cases of H3 (180°), A1-3 (150°), A2-3 (135°), and A3-3 (120°), where positive values represent mid-arch deformation and negative values represent mid-sag deformation. It can be observed from Figure 10 that the peaks of the sagging bending angle are increasing, indicating the accumulation of plastic deformation and buckling as the wave encounters the structure. It can also be seen from Figure 10 that the case of H3 (180°) has a maximum sagging bending angle, which then decreases gradually along with the wave angle. Figure 11 gives the history of the torsional angle in typical oblique waves. It can be seen from Figure 11 that the torsional angle increases with the growth of wave angle, so the case of A3-3 (120°) has a maximum torsional angle.

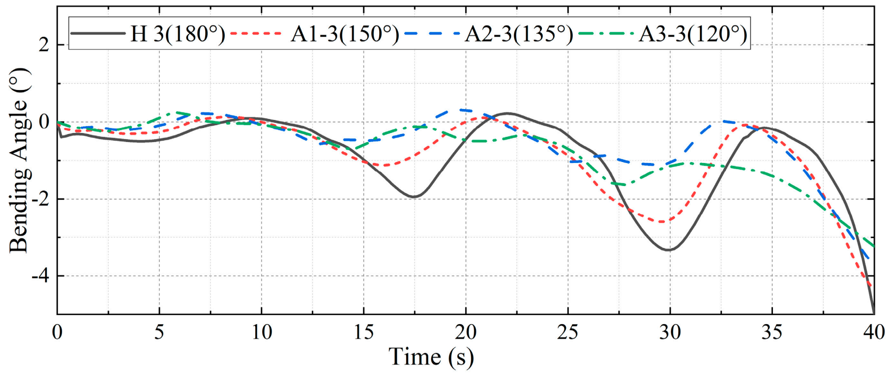

Figure 10. Bending angle deformation of a 4600 TEU containership in large oblique waves.

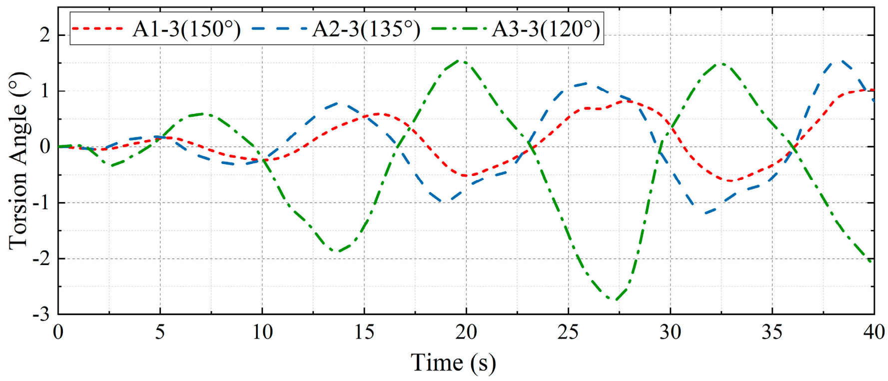

Figure 11. Torsional angle deformation of a 4600 TEU containership.

4.2. Time-Domain Stress History

Five stress points are selected on the midship structure to generate the time-domain stress history, as illustrated in Figure 12. Point 1 is situated at the center of the deck, Point 2 is situated on the upper side of the structure, Point 3 is near the center of the molded depth, Point 4 is positioned on the ship, and Point 5 is located on the ship's bottom. Therefore, the five stress points almost cover the midship section, which is a critical area for structural collapse.

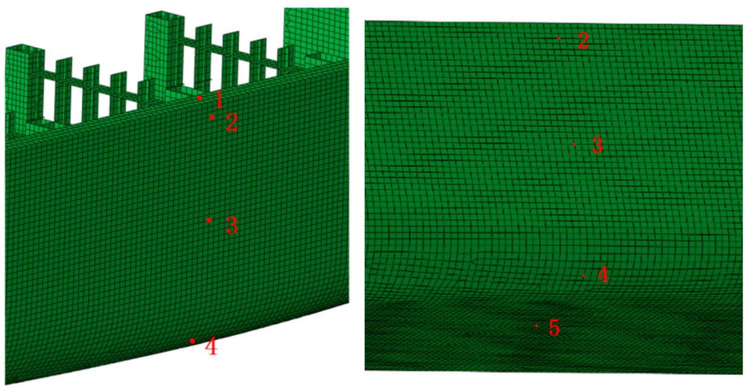

Figure 12. Stress points of a 4600 TEU containership.

The time-domain stress history of the five stress points is outputted in Figure 13. Figure 13a reveals the stress history of the five points for Case H3, which is a wave angle of 0°. Figure 13b gives the stress history of Case A1-3 (150°), Figure 13c presents the stress history of Case A2-3 (135°), and Figure 13d shows the stress history of Case A3-3 (120°). It can be observed from Figure 13a–d that the five stress points reach plasticity in all four cases, which means that the four cases almost cause the containership to collapse. It can be seen from Figure 13a that Points 1, 2, and 5 have stable platform curves with a maximum value equal to yield stress, which indicates that plasticity is generated. Points 1 and 5 have longer plasticity because they are located at the ship deck and ship bottom, where it is easy to cause plasticity. The stability of the platform curve is weakened gradually in Figure 13b–d. It is analyzed that wave angle brings out torsional moment, which weakens the stability of the platform curve, reduces total stress, and causes irregularity to appear.

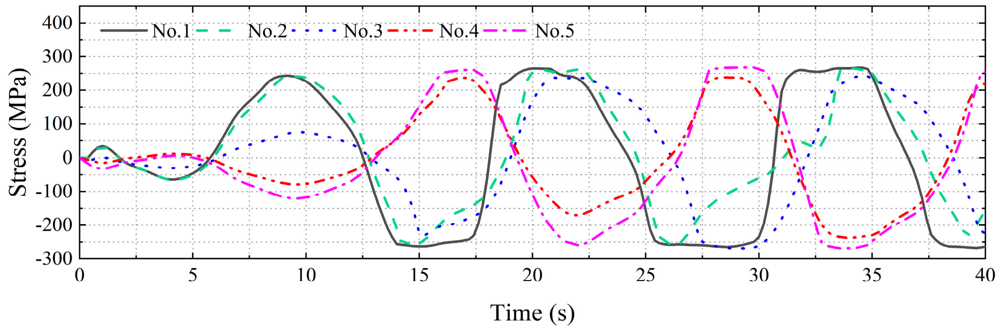

(**a**)

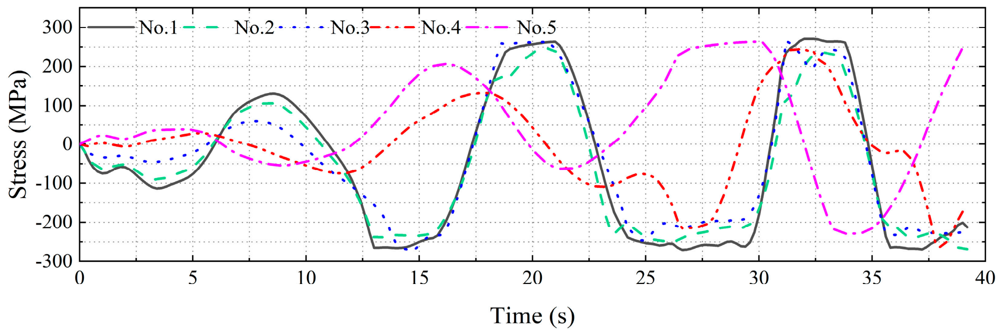

(**b**)

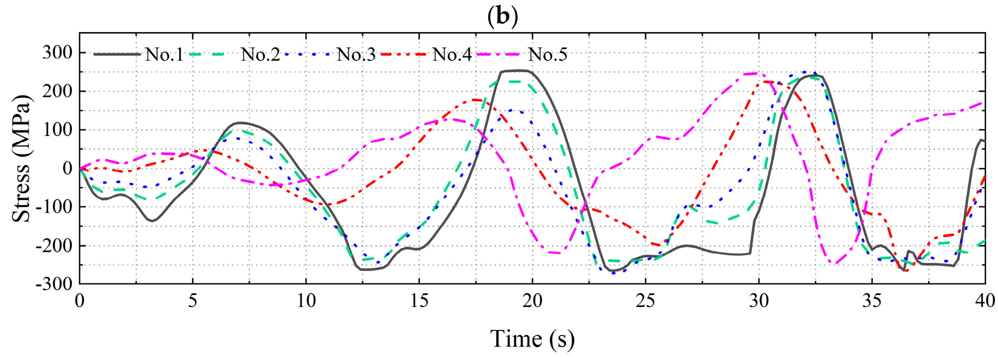

(**c**)

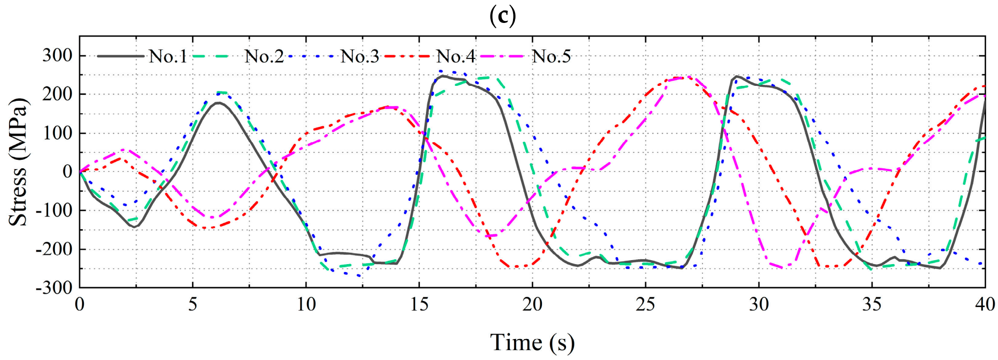

(**d**)

Figure 13. Stress histories of the five stress points. (**a**) Stress history of Case H3. (**b**) Stress history of Case A1-3. (**c**) Stress history of Case A2-3. (**d**) Stress history of Case A3-3.

Furthermore, time-domain analysis reveals that the stress at each measuring point within the container fluctuates periodically. It oscillates between positive and negative values in conjunction with the peaks and troughs of the waves. The size of the cycle is correlated with the period of wave encounters. Figure 13 outputs Von Mises stress, which may exceed the yield strength of 235 MPa to determine whether the structure is yielding. The Von Mises stress is synthetic, so it is larger than the yield strength.

4.3. Time-Domain History of VBM and Torsional Moment

The two-way FSI coupling of CFD and nonlinear FEM is employed to compute the structural collapse of a 4600 TEU containership. Both vertical bending moment (VBM) and torsional moment are taken into account, and they interact with each other. As a result, the VBM and torsional moment of the midship are calculated and analyzed. Figure 14 depicts the VBM history at the midship for the four wave cases. It is evident from Figure 14 that the H3 case at 180° exhibits the highest VBM peaks, and the VBM peak values gradually decrease with the increase in wave angle. This suggests that the heading angle of oblique waves will decrease the VBM peak. Figure 15 presents the history of the torsional moment of midship for three oblique-wave cases. It can be observed from Figure 15 that Case A3-3 (120°) has the largest value of torsional moment, and the torsional moment increases with the growth of wave angle. It is analyzed that the pressure asymmetry between the portside and starboard is stronger as the wave heading angle increases, so the torsional moment is increased. A VBM history from Figure 14 and a torsional moment history from Figure 15 are compared for the same wave case, and it is found that the VBM peak and torsional moment peak are not generated at the same time moment. There is a significant time-phase difference.

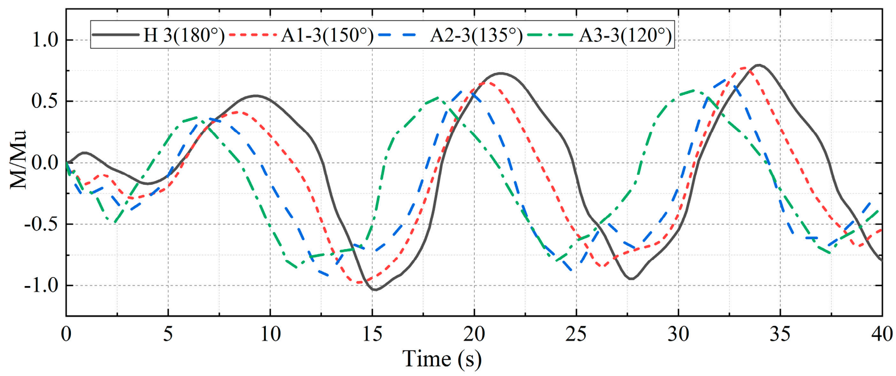

Figure 14. VBM histories of VBM history in the four wave cases.

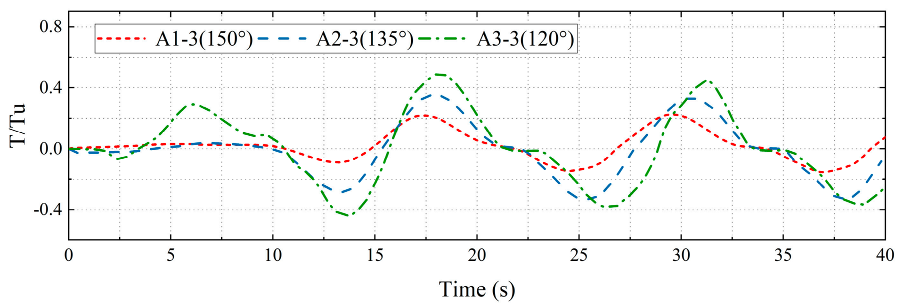

Figure 15. History of the torsional moment of midship for three oblique-wave cases.

4.4. Analysis of Collapsed Course of Typical Oblique Waves

Case A2-3 (wave angle = 135°, wave height = 16 m) is regarded as a typical oblique-wave case. The course of structural collapse is discussed in order to analyze the structural collapse caused by oblique waves. Table 5 shows a structural collapsed nephogram of bending and torsional deformation, as well as the CFD model of a 4600 TEU containership at various time intervals: 12.8 s, 20.2 s, 25 s, 31.8 s, and 37.8 s. It is observed from each row of Table 5 that bending collapse and torsional collapse take place in combination, so a kind of unsymmetrical stress distribution and instability is caused. It is analyzed from the CFD nephogram that when the containership encounters an oblique wave of 45°, it means that there is unsymmetrical pressure distribution on the ship hull so that bending collapse and torsional collapse are combined. It is found from each row of Table 5 that sagging bending and hogging bending occur alternately, but collapse grows worse over time. It can also be seen that left-handed torsion and right-handed torsion take place alternately, and collapse grows worse over time. The overall collapse is reviewed, and it is found that the actual collapsed position is slightly different from the case at 180°. The collapsed position occurred in the midship's front part. It is analyzed that torsion combines with and influences the bending and finally causes the midship front part to collapse. It can be seen from each row of the CFD nephogram that there are obvious wrinkles on the outer surface of the CFD model, which means that the two-way FSI is realized, and the structural deformation solved from the nonlinear FEM is transferred to the CFD model successfully. It can also be seen that the green water is significant as the structural collapse progresses.

Table 5. Structural collapsed nephogram of FEM models and CFD models.

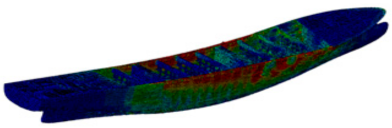 Bending deformation (t = 12.8 s)	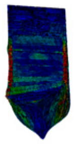 Torsional deformation (t = 12.8 s)	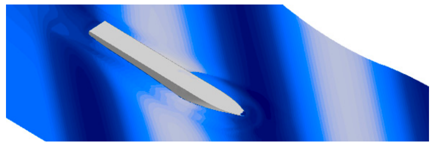 CFD model (t = 12.8 s)
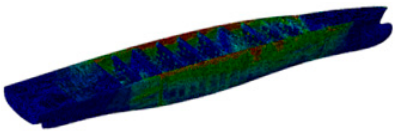 Bending deformation (t = 20.2 s)	 Torsional deformation (t = 20.2 s)	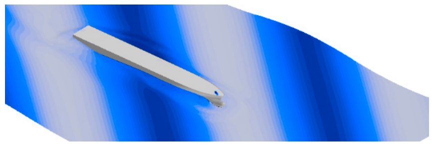 CFD model (t = 20.2 s)
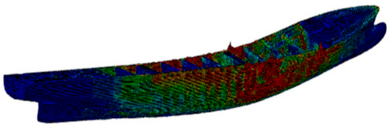 Bending deformation (t = 25 s)	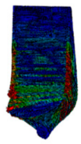 Torsional deformation (t = 25 s)	 CFD model (t = 25 s)
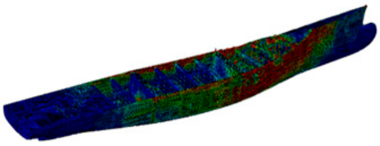 Bending deformation (t = 31.8 s)	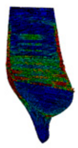 Torsional deformation (t = 31.8 s)	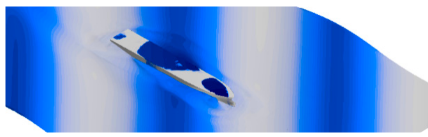 CFD model (t = 31.8 s)
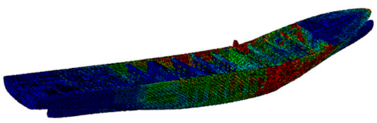 Bending deformation (t = 37.8 s)	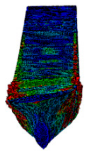 Torsional deformation (t = 37.8 s)	 CFD model (t = 37.8 s)

5. Discussion

Based on the overall research results, the extensive discussion of hydroelasto-plastic results is carried out by changing the wave height, wave angle, and wave height.

First, the bending and torsional deformation of the midship is discussed by increasing the wave height. Figure 16a illustrates the maximum bending rotational deformation of the midship as wave height changes and Figure 16b shows the maximum torsional angle of the midship as wave height changes. It is observed that the maximum bending, rotational, and torsional deformations increase with the growth of wave height. The increase in deformation is nonlinear, so a wave height of 16 m results in significant nonlinear deformation. This indicates that a wave height of 16 m could potentially cause the collapse of the ship structure, as shown in Figure 16. Figure 17 illustrates the maximum bending rotational and torsional deformations of the midship as the wave angle changes. Figure 17a shows the maximum bending rotational deformation as the wave angle changes, while Figure 17b depicts the maximum torsional deformation as the wave angle changes. It is observed that the maximum bending rotational deformation decreases slightly as the wave angle increases, as shown in Figure 17a. Additionally, Figure 17b indicates that the maximum torsional angle increases with the growth of the wave angle. This suggests that oblique waves can reduce the longitudinal bending strength.

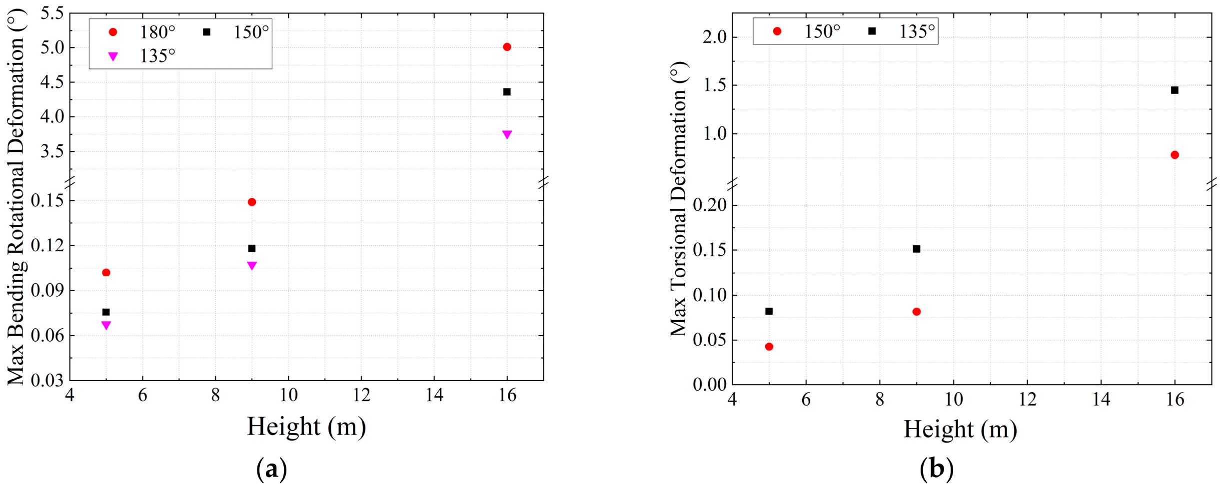

Figure 16. Maximum bending rotational and torsional deformation of the midship by changing wave height. (**a**) Maximum bending rotational deformation. (**b**) Maximum torsional deformation.

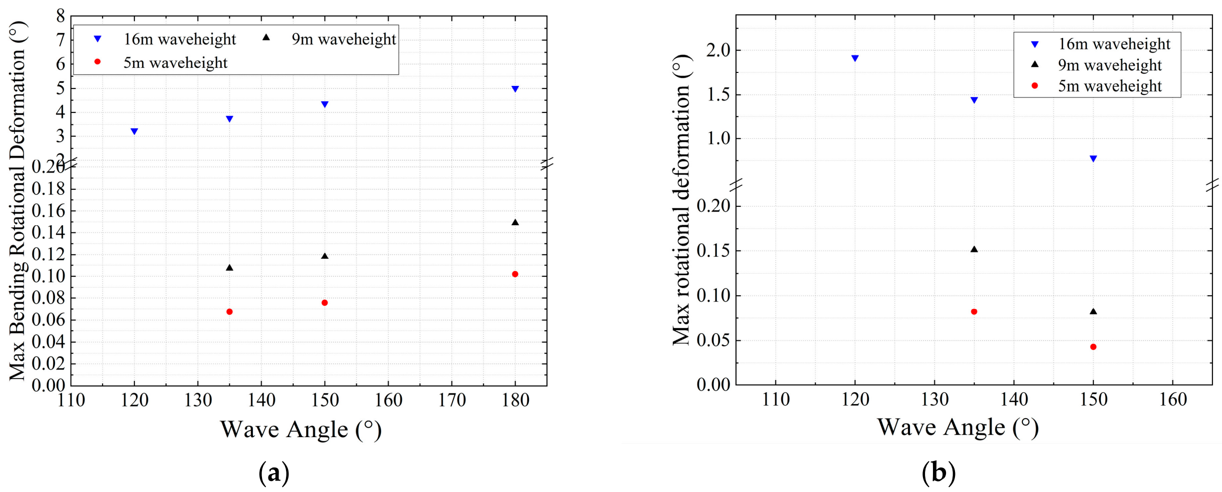

Figure 17. Maximum bending rotational and torsional deformation of midship by changing wave angle. (**a**) Maximum bending rotational deformation. (**b**) Maximum torsional deformation.

Second, the maximum bending moment and torsional moment at midship are discussed when the ship is floating in oblique waves. Figure 18a illustrates the maximum bending moment as a function of changing wave height. The vertical axis represents the ratio of the maximum bending moment to the ultimate bending moment, where a ratio of 1 indicates that the ship structure has reached the ultimate bending moment and the ship has collapsed. It is evident from Figure 18a that the maximum bending moment increases with the growth of wave height. Figure 18b demonstrates the maximum torsional moment increasing with wave height. The vertical axis represents the ratio of the maximum torsional moment to the ultimate torsional moment. It can be observed from Figure 18b that the maximum torsional moment increases with the growth of wave height. Figure 19 discusses the maximum bending moment and torsional moment at midship by varying the wave angle. Subfigure (a) shows the maximum bending moment, and subfigure (b) presents the torsional moment with changing wave angle. It can be observed that the maximum bending moment slightly decreases with increasing wave angle, as shown in Figure 19a. Additionally, it is evident from Figure 19b that the maximum torsional moment increases with the growth of the wave angle. This indicates that oblique waves generate both bending and torsional moments. The torsional moment leads to a slight decrease in the bending moment. Therefore, it is important to discuss their combined effect.

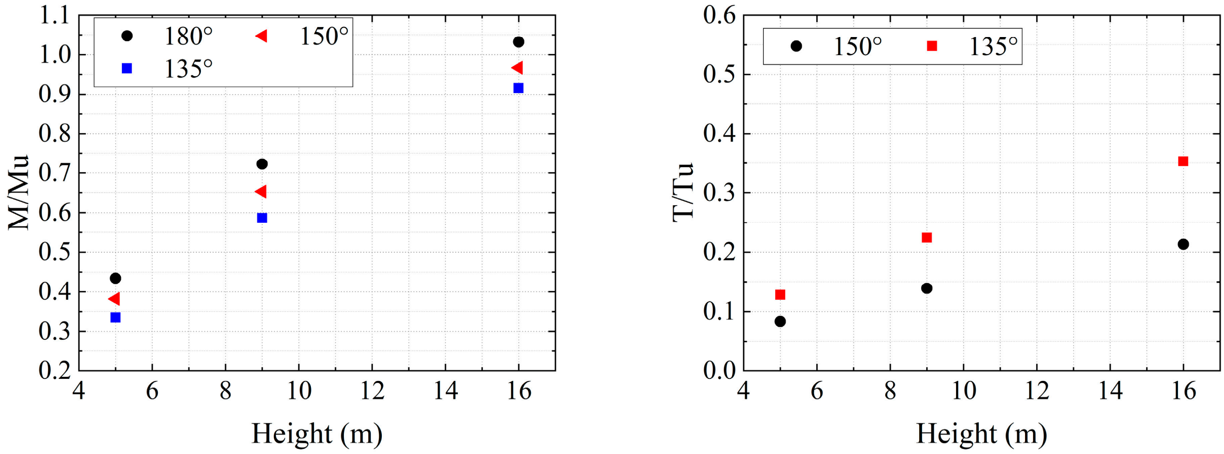

(**a**) (**b**)

Figure 18. Maximum bending moment and torsional moment of midship by changing wave height. (**a**) Maximum bending moment. (**b**) Maximum torsional moment.

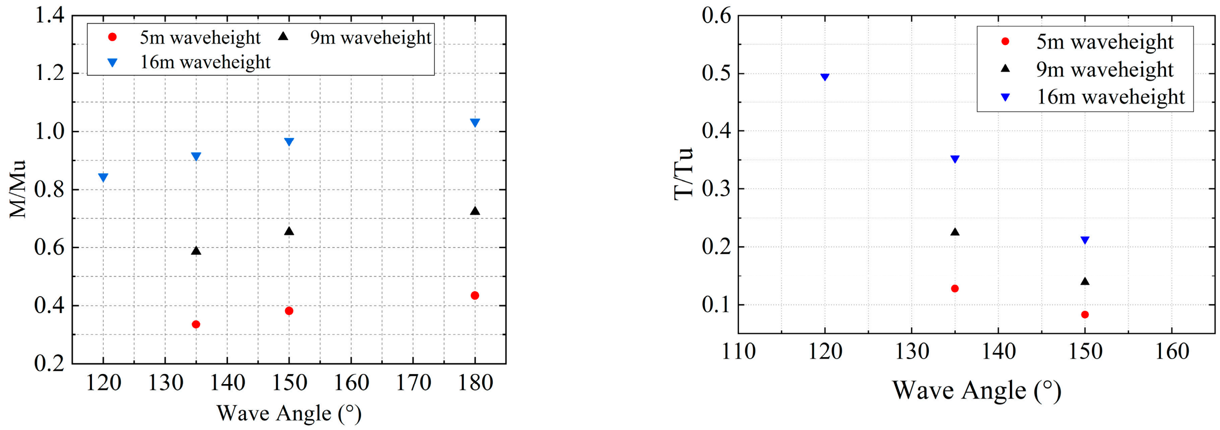

(**a**) (**b**)

Figure 19. Maximum bending moment and torsional moment of midship by changing wave angle. (**a**) Maximum bending moment. (**b**) Maximum torsional moment.

The elliptic relationship between bending moment and torque at the midship is shown in Figure 20. The vertical axis represents the maximum bending moment, and the horizontal axis denotes the maximum torsional moment at the point of collapse. Five collapsed cases involving wave angles of 100°, 120°, 135°, 150°, and 180° are selected to discuss the combined effect of bending moment and torsional moment. In Figure 20, five points are plotted, forming a quarter of an ellipse. The ellipse represents the variation of the bending moment and torsional moment by changing wave angles. It is evident from Figure 20 that the structural bending moment decreases as the wave angle increases, accompanied by an increase in the torsional moment, demonstrating an elliptical coupling.

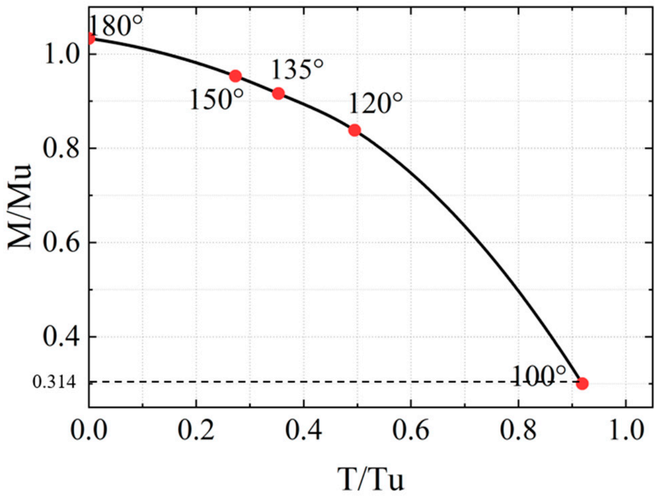

Figure 20. Elliptic coupling of bending moment and torque in midship.

6. Conclusions

This paper studies the structural collapse of a 4600 TEU containership caused by oblique waves. A numerical hydroelasto-plastic coupling of CFD and nonlinear FEM was used to study the structural collapse of a containership in oblique waves. Several oblique-wave cases involving heading angles of 120°, 135°, 150°, and 180° were determined and calculated. Typical cases are studied for time-domain histories and collapse courses, then the overall results are discussed. Four conclusions are obtained as follows:

(1) One of the innovations of this paper is to propose a numerical hydroelasto-plastic coupling of CFD and nonlinear FEM, which can evaluate the structural collapse of a full-scale containership considering the coupling of bending moment and torsional moment.

(2) The collapse of a containership appears to be a combination of bending and torsion; it can be observed that as torsions take place, collapse grows worse. The combined collapse is very different from the heading collapse of a ship.

(3) Oblique waves cause both bending and torsional moments. The torsional moment reduces the ultimate bending moment to a certain extent.

The numerical 3D hydroelasto-plastic approach and numerical results will be performed to simulate the hydroelasto-plastic model experiment.

Author Contributions: Methodology, Y.Z.; Software, Q.Z.; Validation, Y.N.; Supervision, W.L. and X.S. All authors have read and agreed to the published version of the manuscript.

Funding: This work was funded by the National Key Research and Development Project (No.: 2022YFC3006001), the National Natural Science Foundation of China (No.: 52071243, 52101371), and the Wuhan Science and Technology Plan Project (2023010402010602).

Institutional Review Board Statement: Not applicable.

Informed Consent Statement: Not applicable.

Data Availability Statement: Data are contained within the article.

Conflicts of Interest: Author Yong Nie was employed by the company China Harzone Industry Corp., Ltd. The remaining authors declare that the research was conducted in the absence of any commercial or financial relationships that could be construed as a potential conflict of interest.

References

1. Kim, K.; Yoo, H.C. Ultimate strengths of steel rectangular box beams subjected to combined action of bending and torsion. *Eng. Struct.* **2008**, *30*, 1677–1687. [CrossRef]
2. Wang, Q.; Wang, D. Ultimate strength envelope of a 10,000 TEU large container ship subjected to combined loads: From compartment model to global hull girder. *Ocean Eng.* **2020**, *213*, 107767. [CrossRef]
3. Muller, P.; Garrett, C.; Osborne, A.L. Rogue wave. *Oceangraphy* **2005**, *18*, 66–75.
4. Update on incident involving the containership MOL Comfort. *Am. J. Transp.* **2013**.
5. Koh, T.J.; Paik, J.K. Structural failure assessment of a post-Panamax class containership: Lessons learned from the MSC Napoli accident. *Ships Offshore Struct.* **2015**, *11*, 847–859. [CrossRef]
6. Group, F.W. Urea cargo ship sinks in Black Sea killing three. *Fertilizer Week* **2021**, 21.
7. Ostapenko, A.; Vaucher, A. *Ultimate Strength of Ship Hull Girders under Moment, Shear and Torque*; Report No. 453.6; Fritz Engineering Laboratory, Lehigh University: Bethlehem, PA, USA, 1980.
8. Ostapenko, A. Strength of ship hull girders under moment, shear and torque. In Proceedings of the Extreme Loads Response Symposium, SSC-SNAME, Arlington, VA, USA, 19–20 October 1981.
9. Ostapenko, A.; Moore, T.R. *Maximum Strength of Ship Hulls Subjected to Moment, Torque and Shear*; Report No. 479.5; Fritz Engineering Laboratory, Lehigh University: Bethlehem, PA, USA, 1982.
10. Pedersen, P.T. Beam theories for torsional-bending response of ship hulls. *J. Ship Res.* **1991**, *35*, 254–265. [CrossRef]
11. Paik, J.K.; Thayamballi, A.K.; Pedersen, P.T.; Park, Y.I. Ultimate strength of ship hulls under torsion. *Ocean Eng.* **2001**, *28*, 1097–1133. [CrossRef]
12. Sun, H.H.; Guedes Soares, C. An experimental study of ultimate torsional strength of a ship-type hull girder with a large deck opening. *Mar. Struct.* **2003**, *16*, 51–67. [CrossRef]
13. Tanaka, Y.; Ogawa, H.; Tatsumi, A.; Fujikubo, M. Analysis method of ultimate hull girder strength under combined loads. *Ships Offshore Struct.* **2015**, *10*, 587–598. [CrossRef]
14. Wang, C.; Wu, J.; Wang, D. Design similar scale model of a 10,000 TEU container ship through combined ultimate longitudinal bending and torsion analysis. *Appl. Ocean Res.* **2019**, *88*, 1–14. [CrossRef]
15. Zhong, Q.; Wang, D. Numerical investigation on ultimate strength of sandwich box girders under vertical bending and torsion. *Ocean Eng.* **2022**, *254*. [CrossRef]
16. Lee, D.H.; Paik, J.K. Ultimate strength characteristics of as-built ultra-large containership hull structures under combined vertical bending and torsion. *Ships Offshore Struct.* **2020**, *15*, S143–S160. [CrossRef]
17. Hu, K.; Yang, P.; Xia, T. Residual ultimate strength of large opening box girder with crack damage under torsion and bending loads. *Ocean Eng.* **2018**, *162*, 274–289. [CrossRef]
18. Hirdaris, S.E.; Price, W.G.; Temarel, P. Two- and Three-Dimensional Hydroelastic Modeling of a Bulker in Regular Waves. *Mar. Struct.* **2003**, *16*, 627–658. [CrossRef]
19. Robert, M.; Monroy, C.; Reliquet, G.; Drouet, A.; Ducoin, A.; Guillerm, P.E.; Ferrant, P. Hydroelastic response of a flexible barge investigated with a viscous flow solver. In Proceedings of the 7th International Conference on Hydroelasticity in Marine Technology-Hydroelasticity'15, Split, Croatia, 16–19 September 2015.
20. Seng, S.; Jensen, J.J.; Malenica, Š. Global hydroelastic model for springing and whipping based on a free-surface CFD code (OpenFOAM). *Int. J. Nav. Archit. Ocean. Eng.* **2014**, *6*, 1024–1040. [CrossRef]
21. Lin, Y.; Ma, N.; Gu, X. Experimental study on the asymmetric impact loads and hydroelastic responses of a very large container ship. *Int. J. Nav. Archit. Ocean Eng.* **2020**, *12*, 226–240. [CrossRef]
22. Kim, S. Experimental investigation on wave-induced bending moments of a 6750-TEU containership in oblique waves. *Ocean. Eng.* **2023**, *284*, 115161. [CrossRef]
23. Ivo, S.; Vladimir, N.; Tomic, M. Some aspects of structural modelling and restoring stiffness in hydroelastic analysis of large container ships. *Ships Offshore Struct.* **2014**, *9*, 199–217.
24. Zhu, S.; Wu, M.K.; Moan, T. Experimental investigation of hull girder vibrations of a flexible backbone model in bending and torsion. *Appl. Ocean Res.* **2011**, *33*, 252–274. [CrossRef]
25. Kim, Y.; Kim, K.H.; Kim, Y. Analysis of Hydroelasticity of Floating Shiplike Structure in Time Domain Using a Fully Coupled Hybrid BEM-FEM. *J. Ship Res.* **2009**, *53*, 31–47. [CrossRef]
26. Sun, Q.; Zhou, H.; Gu, Q. Study on the Wave Loads and Structural Stresses of Container Ship. *J. Phys. Conf. Ser.* **2018**, *1064*, 012033. [CrossRef]
27. Riesner, M.; Moctar, O.E. A numerical method to compute global resonant vibrations of ships at forward speed in oblique waves. *Appl. Ocean Res.* **2021**, *108*, 102520. [CrossRef]
28. Masaoka, K.; Okada, H. A Numerical Approach for Ship Hull Girder Collapse Behavior in Waves. In Proceedings of the International Offshore and Polar Engineering Conference, Honolulu, HI, USA, 25–30 May 2003.
29. Xu, W.; Iijima, K.; Wada, R. Experimental evaluation of the post-ultimate strength behavior of a ship's hull girder in waves. *J. Mar. Sci. Appl.* **2012**, *17*, 34–43. [CrossRef]
30. Liu, W.; Song, X.; Wu, W. Strength of a Containership in Extreme Waves Obtained by Nonlinear Hydroelasto-plasticity Dynamic analysis and Finite Element Modeling. *J. Offshore Mech. Arct. Eng.* **2016**, *138*, 031602. [CrossRef]

31. Lakshmynarayanana, P.; Temarel, P.; Chen, Z. Hydroelastic analysis of a flexible barge in regular waves using coupled CFD-FEM modelling. *Anal. Des. Mar. Struct.* **2015**, 95–103.
32. Pal, S.K.; Iijima, K. Investigation of Springing Responses to High Harmonics of Wave Loads by Direct Coupling between CFD and FEM. In Proceedings of the ASME 2022 41st International Conference on Ocean, Offshore and Arctic Engineering, Hamburg, Germany, 5–10 June 2022.
33. Liu, W.; Luo, W.; Xia, T. Development of a Fully Coupled Numerical Hydroelasto-plastic Approach for Offshore Structure. *Ocean Eng.* **2022**, *258*, 111713. [CrossRef]
34. Tezdogan, T.; Demirel, Y.K.; Kellett, P.; Khorasanchi, M.; Incecik, A.; Turan, O. Full-scale unsteady RANS CFD simulations of ship behaviour and performance in head seas due to slow steaming. *Ocean Eng.* **2015**, *97*, 186–206. [CrossRef]
35. ITTC Recommended Procedures and Guidelines: Practical Guidelines for Ship CFD Applications. 2011. Available online: https://ittc.info/media/1357/75-03-02-03.pdf (accessed on 25 December 2023).